

# Experimental Determination of Complex Optical Constants of Air-Stable Inorganic CsPbI<sub>3</sub> Perovskite Thin Films

Wensheng Yan,\* Yi Guo, Deski Beri, Stephan Dottermusch, Haining Chen,\* and Bryce S. Richards

Air-stable inorganic cesium lead iodide (CsPbI<sub>3</sub>) perovskite thin films with a bandgap of 1.7 eV are a promising candidate for tandem cell solar cells, comprising a perovskite top cell with a crystalline silicon bottom cell. The device design and simulations are important to develop high-efficiency photovoltaic devices. However, knowledge of complex optical constants of the CsPbI<sub>3</sub> thin films is mandatory to complement such tasks. Herein, air-stable inorganic CsPbI<sub>3</sub> perovskite thin films are prepared using one-step synthesis through a spin-coating method. Variable angle spectroscopic ellipsometry (VASE) is then conducted at five angles (43.9°, 48.9°, 53.9°, 58.9°, and 63.9°) to obtain ellipsometric data ( $\Psi$  and  $\Delta$ ). The thickness nonuniformity model of the perovskite thin film combined with an effective medium approximation for describing rough surface is adopted to achieve excellent fitting. The complex optical constants of the CsPbI<sub>3</sub> thin film are experimentally obtained in the wavelength range of 300–1200 nm. The present results open the door for design and simulations on high-efficiency CsPbI<sub>3</sub>/c-Si tandem solar cells.

The power conversion efficiency (PCE) of the organic–inorganic hybrid perovskite solar cells (PSCs) based on lead halides progressed rapidly from 3.8% in 2009 to 24.2% in 2019.<sup>[1,2]</sup> In recent years, all-inorganic perovskite thin films for solar cells have

attracted great attention due to significantly improved stability compared with organic-containing perovskites.<sup>[3–5]</sup> Although the PCE of all-inorganic perovskite solar cells lags somewhat behind, excellent progress is being made with the best devices reaching 18% PCE.<sup>[6–10]</sup>

Among all-inorganic perovskite solar cells, those based on CsPbI<sub>3</sub> perovskite ( $\alpha$ ,  $\beta$ , or  $\gamma$  phases) thin films are particularly attractive due to the optical bandgap lying in the range of 1.68–1.73 eV.<sup>[11–17]</sup> This means that CsPbI<sub>3</sub> perovskite thin films are well suited for the development of ultrahigh-efficiency tandem cells, whereby a perovskite top cell is partnered together with a low-bandgap ( $\approx$ 1.1 eV) solar cell such as crystalline silicon (c-Si). However, realizing air-stable CsPbI<sub>3</sub> perovskite thin films remains a challenge at present.

This is because a typical CsPbI<sub>3</sub> perovskite exhibits a thermodynamic instability at room temperature and transforms spontaneously and very quickly (within a matter of minutes) from black perovskite ( $\alpha$ ,  $\beta$ , or  $\gamma$  phase) into the undesirable yellow-phase CsPbI<sub>3</sub> ( $\delta$ -CsPbI<sub>3</sub>) in air.<sup>[13,18]</sup> So far, several groups have investigated the structural phases of CsPbI<sub>3</sub> perovskite.<sup>[10,18–20]</sup> It was reported that black perovskite  $\beta$ -CsPbI<sub>3</sub> and  $\gamma$ -CsPbI<sub>3</sub> are distorted phases, which are slightly splitted relative to the  $\alpha$ -CsPbI<sub>3</sub> phase.<sup>[20]</sup> In contrast to the yellow  $\delta$  phase consists of double-chains of noncorner-sharing [PbI<sub>6/2</sub>]<sup>−</sup> octahedral, the three black phases of  $\alpha$ ,  $\beta$ , and  $\gamma$  show obviously corner-sharing [PbI<sub>6/2</sub>]<sup>−</sup> octahedral.<sup>[20]</sup>


It is well known that the optical design and optimization to achieve the minimum optical losses are important to develop high-efficiency perovskite/c-Si tandem devices.<sup>[21–24]</sup> Such investigations can not only provide an effective guide on high-performance device fabrication but also offer an analysis and feedback to the experimental results such as light absorption in the absorber and the resulting photocurrent density and quantum efficiency. These information are also important in designing a light-manipulation structure based on perovskites such as reflector grating, absorber grating, and waveguiding layer.<sup>[25–28]</sup> In addition, the obtained optical simulation results can be used as inputs to an electrical model to predict full device performance.

Before performing such tasks, however, knowledge of complex optical constants of CsPbI<sub>3</sub> perovskite thin films is mandatory. There are already many reports on the determination of the optical constants of organic–inorganic hybrid perovskites.<sup>[29–33]</sup> There are

Dr. W. Yan, D. Beri, Dr. S. Dottermusch, Prof. B. S. Richards  
Institute of Microstructure Technology (IMT)  
Karlsruhe Institute of Technology  
Hermann-von-Helmholtz-Platz 1, Eggenstein-Leopoldshafen 76344,  
Germany  
E-mail: Wensheng.Yan@kit.edu

Y. Guo, Prof. H. Chen  
School of Materials Science and Engineering  
Beihang University  
No. 37 Xueyuan Road, Haidian District, Beijing 100191, P. R. China  
E-mail: Chenhaining@buaa.edu.cn

Prof. B. S. Richards  
Light Technology Institute (LTI)  
Karlsruhe Institute of Technology  
Engesserstrasse 13, Karlsruhe 76131, Germany

 The ORCID identification number(s) for the author(s) of this article can be found under <https://doi.org/10.1002/pssr.202000070>.

© 2020 The Authors. Published by WILEY-VCH Verlag GmbH & Co. KGaA, Weinheim. This is an open access article under the terms of the Creative Commons Attribution-NonCommercial License, which permits use, distribution and reproduction in any medium, provided the original work is properly cited and is not used for commercial purposes.

DOI: 10.1002/pssr.202000070

also some reports regarding all-inorganic perovskite thin films such as CsPbBr<sub>3</sub> and CsPbI<sub>3</sub>.<sup>[34,35]</sup> However, looking into the reported refractive index ( $n$ ) and extinction coefficient ( $k$ ) of CsPbI<sub>3</sub> thin films in ref. [35], it is found that the reliability is low, for example, the  $k$  values are much below zero (minimum  $k$  value is up to about  $-0.25$ ) in the wavelength ( $\lambda$ ) range of 750–1050 nm and 1350–1700 nm. In addition, no any details including the adopted model, fitting parameters, comparison between the ellipsometric data and the fitting results, as well as sample stability were given.<sup>[35]</sup> Because the PCE of CsPbI<sub>3</sub> perovskite solar cells is progressing fast with latest report of up to 18%,<sup>[10,18–20,36]</sup> the experimental determination of the optical constants of CsPbI<sub>3</sub> perovskite thin films is never as urgent as now.

In this work, we experimentally determine the complex optical constants of air-stable inorganic CsPbI<sub>3</sub> perovskite thin films. Air-stable CsPbI<sub>3</sub> perovskite thin films are synthesized using a one-step solution method. Variable angle spectroscopic ellipsometry (VASE) is measured at five angles (43.9°, 48.9°, 53.9°, 58.9°, and 63.9°) to obtain the complex optical constants of the present CsPbI<sub>3</sub> thin films. It is noteworthy that the CsPbI<sub>3</sub> samples in this work were measured under ambient conditions without any encapsulation. This is made possible through the CsPbI<sub>3</sub> perovskite thin film remaining air-stable long enough for the VASE measurements to take place (the VASE measurements take 3 min here). To achieve excellent fitting of the measured

ellipsometric data parameters ( $\Psi$  and  $\Delta$ ), an appropriate model is constructed using commercially available software (WVASE32 v.3.888, J. A. Woollam). Here, we adopt a model of perovskite thin film with nonuniform thickness, where one Tauc–Lorentz (T–L) oscillator and four Gaussian (Gau) oscillators are chosen to describe the bulk CsPbI<sub>3</sub> film and an effective medium approximation (EMA) with the voids of 50% is used to describe rough surface. Finally, the experimental complex optical constants are determined in the wavelength range of 300–1200 nm, which fully covers the spectrum response range of a CsPbI<sub>3</sub>/c-Si tandem cell. The resulting optical constants can be used in optical simulations to explore different photovoltaic device designs based on CsPbI<sub>3</sub> absorbers.

Figure 1a shows the measured X-ray diffraction (XRD) pattern of the prepared CsPbI<sub>3</sub> thin film on the bare glass substrate. The diffraction peaks at 14.34°, 20.68°, 22.98°, 24.07°, 25.18°, 28.94°, 32.35°, and 35.92° correspond to (110), (020), (120), (121), (022), (220), (130), and (132) planes of the  $\gamma$ -CsPbI<sub>3</sub> perovskite. The measured UV–vis absorbance spectrum and photoluminescence (PL) spectrum of the CsPbI<sub>3</sub> thin film are shown in Figure 1b. Through the use of a Tauc plot, the optical bandgap can be estimated from the plotting of  $(Ah\nu)^2$  versus photon energy ( $h\nu$ ), as shown in Figure 1c, where the present CsPbI<sub>3</sub> perovskite thin film exhibits a direct bandgap at 1.738 eV. It is determined from the PL measurement that the peak emission wavelength is

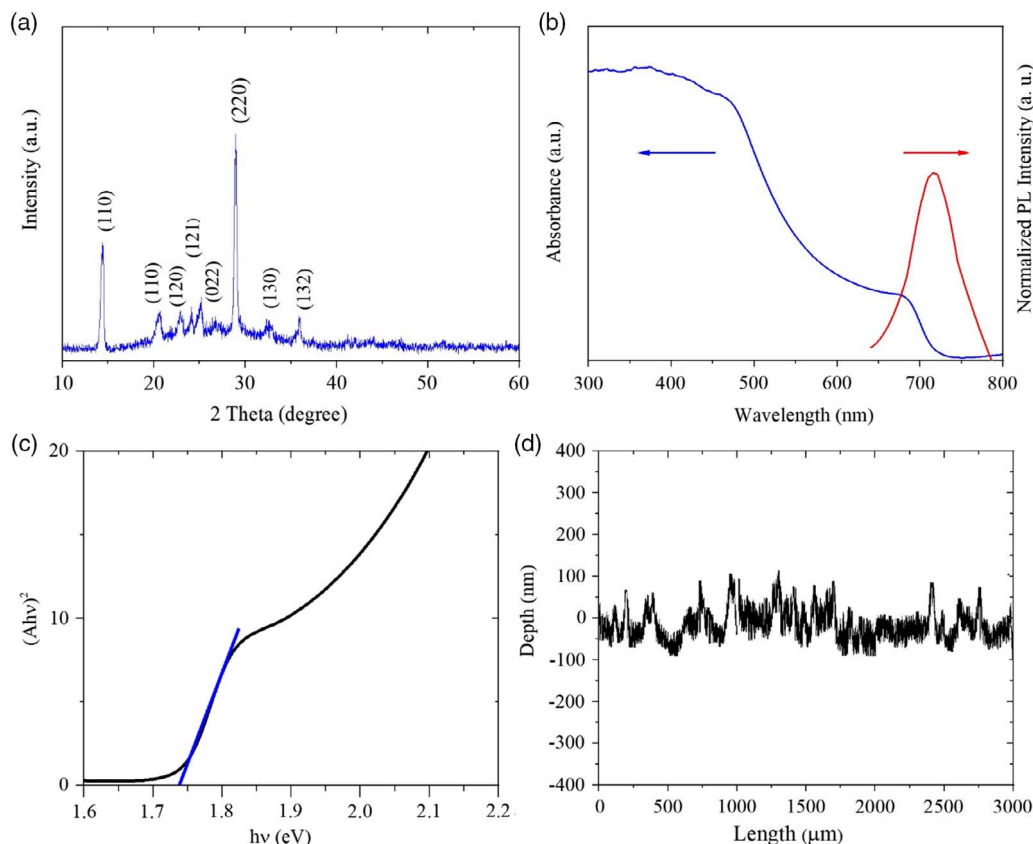


**Figure 1.** a) The XRD pattern of the CsPbI<sub>3</sub> thin film on the bare glass substrate. b) The measured wavelength-dependent absorbance of the present perovskite thin film and PL measurement. c) The Tauc plotting for estimating optical bandgap of the perovskite thin film. d) CsPbI<sub>3</sub> surface profile across the ellipsometry measurement region.

around 718 nm, which is close agreement with the optical bandgap estimated from the absorbance spectrum (Figure 1c). Figure 1d shows CsPbI<sub>3</sub> surface profile across the ellipsometry measurement region, where the shown scan length is 3000 μm (note that the size of beam spot is in a diameter of 200 μm). Figure 1d shows that the present CsPbI<sub>3</sub> thin film is not uniform in terms of thickness. More evidence regarding the nonuniform thickness will be subsequently presented by using cross-sectional scanning electron microscopy (SEM) images. It means that the thickness nonuniformity model should be considered to fit the ellipsometric data for generating complex optical constants.

The measured thin film thickness and surface roughness of the CsPbI<sub>3</sub> thin film through the cross-sectional SEM and surface atomic force microscope (AFM) are shown in Figure 2. In the current work, the surface roughness defines vertical root-mean-square roughness. As shown in Figure 2a,b, it can be seen from two SEM images taken at two locations of the same sample that the thicknesses are quite different. Combining Figure 1d, these facts indicate the thickness of the present thin film is not uniform. Based on the measurements, the estimated bulk thickness of the CsPbI<sub>3</sub> thin film is 500 nm (uncertainty: ±25 nm) and the thickness variation is 14% (uncertainty: ±2%). Figure 2c shows a surface AFM image for the region of 2 × 2 μm, where the surface roughness value is 15 nm.

It is found that even under a normal environment (room temperature and humidity of 60%), the present CsPbI<sub>3</sub> perovskite thin films can remain stability of structure for up to 15–20 min, which offers a sufficient time window to finish the VASE measurement (only 3 min) and thus avoiding the need for sample encapsulation to prevent sample from degrading. Figure 3a shows a schematic of a perovskite thin film of nonuniform thickness on a glass substrate (note that here the drawing of nonuniform thickness is not scalable and just is used for a model illustration). Figure 3b is the chosen model to fit the measured ellipsometric data ( $\Psi$  and  $\Delta$ ). Through the optimization, it is found the best fitting results are as follows: nonuniform thickness variation is 11.8% for the perovskite thin film, where this thickness variation is a fitting parameter during the optimization; one T–L oscillator and four Gau oscillators are used to describe the bulk CsPbI<sub>3</sub> thin film; and an EMA with a  $x = 50\%$  void component is used to describe the rough surface of the perovskite thin film. During the aforementioned simulations, a square

convolution profile shape was adopted, which is based on the cross-sectional SEM images measured. If the triangular or Gau profile shapes are used for a replacement of square, the obtained wavelength-dependent complex optical constants are not affected. It means that the present case is not sensitive to these three kinds of shapes. The measured and fitted  $\Psi$  and  $\Delta$  are shown in Figure 3c,d in the wavelength range of 300–1200 nm, respectively. It can be seen that very good fitting results are achieved for both  $\Psi$  and  $\Delta$ . The average thickness of the perovskite thin film and surface roughness extracted from the fitting results are 468 and 9 nm, respectively. Finally, the obtained parameters from the best fitting and the estimated values from the measurements are shown in Table 1. It is found that the surface roughness is  $15 \pm 3$  nm, which is estimated from the AFM measurement. This value is higher than the fitting result of 9 nm. The bulk thickness of the perovskite thin film from the cross-sectional SEM images is  $500 \pm 25$  nm. The fitted bulk thickness of the CsPbI<sub>3</sub> thin film is 468 nm. Regarding the nonuniformity variation of CsPbI<sub>3</sub> thin film, the estimated nonuniformity variation from SEM measurement is  $14 \pm 2\%$ , whereas the fitted value of nonuniformity variation is 12%. If the measurement uncertainty is considered, a good agreement is shown between the fitting results and measurements.

From the aforementioned, we can obtain the dispersive  $n$  and  $k$  values in wavelength range of 300–1200 nm. The result is shown in Figure 4, where the results from a literature are included to conduct a comparison. Ref. [35] reported the angle-dependent complex optical constants of CsPbI<sub>3</sub> perovskite thin film at incident angles of 55°, 60°, 65°, and 70°. However, this literature neither gave any details regarding the adopted model and fitting parameters nor gave reasons why their complex optical constants are dependent of incident angles. In general, the complex optical constants of a material, for example, a perovskite thin film, should be independent of incident angles. For a comparison, the  $n$  and  $k$  values in the wavelength of 400–1200 nm at the two angles of 55° and 70° in ref. [35] are shown in Figure 4. The values of optical constants at the other two angles of 60° and 65° in ref. [35] are not plotted because they are between that at the two angles of 55° and 70°. In contrast to ref. [35], our complex optical constants are independent of incident angle and this is normal. In addition, our  $n$  values are much higher than that of ref. [35] except for the values at the wavelength

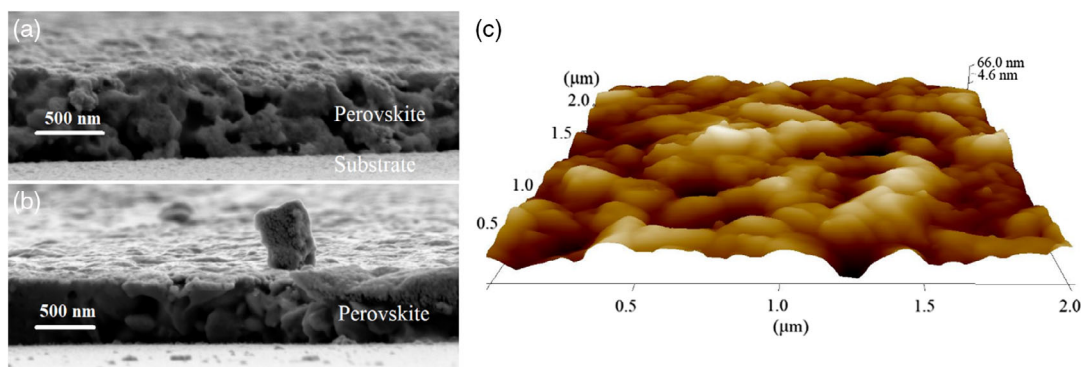


**Figure 2.** a,b) Two SEM images of the CsPbI<sub>3</sub> thin film taken at different locations. c) The surface AFM image of the CsPbI<sub>3</sub> thin film with an area of 2 μm × 2 μm.

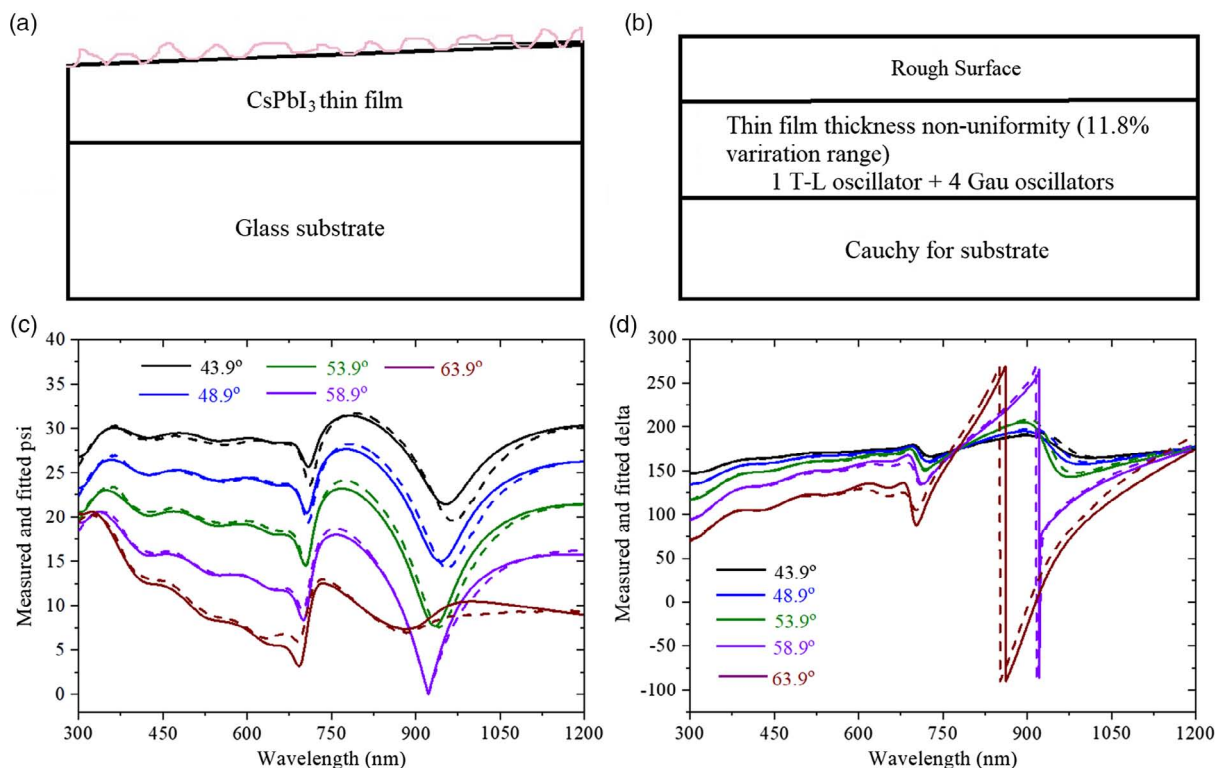


**Figure 3.** a) Schematic diagram of the present sample structure (not to scale). b) Constructed model for the fitting. c) The measured and fitted  $\psi$  ( $\Psi$ ) at the five angles of  $43.9^\circ$ ,  $48.9^\circ$ ,  $53.9^\circ$ ,  $58.9^\circ$ , and  $63.9^\circ$ . d) The measured and fitted  $\Delta$  at the angles of  $43.9^\circ$ ,  $48.9^\circ$ ,  $53.9^\circ$ ,  $58.9^\circ$ , and  $63.9^\circ$ .

**Table 1.** The extracted parameters from the best fitting to ellipsometric data and the estimated values from the measurements.

$d_{\text{rough}}$	9 nm (fitting result)	$15 \pm 3$ nm (estimated from AFM)			
$d_{\text{bulk}}$	468 nm (fitting result)	$500 \pm 25$ nm (estimated from SEM)			
Nonuniformity variation	12% (fitting result)	$14 \pm 2\%$ (estimated from SEM)			
Oscillator parameters from the best fitting					
Oscillators	$A_n$	$E_n$ or $E_{0n}$ [eV]	$C_n$ [eV]	$E_{gn}$ [eV]	$B_{rn}$ [eV]
1: T-L	23.91 eV	1.82	0.20	1.69	–
2: Gau	2.23	2.67	–	–	0.58
3: Gau	0.59	2.16	–	–	0.34
4: Gau	3.97	3.41	–	–	0.80
5: Gau	2.43	4.34	–	–	1.01

of 440 nm. In terms of extinction coefficient, it is seen from Figure 4 that in our case, the  $k$  values become zero when the wavelength is greater than around 718 nm. In contrast, it is surprising to see that  $k$  values get minus (up to  $-0.25$ ) at the wavelength range of 750–1050 nm for incident angle of  $55^\circ$  and the wavelength range of 840–990 nm for incident angle of  $70^\circ$ . It indicates that the  $n$  and  $k$  results reported in ref. [35] are in a low reliability. In contrast, the minimum  $k$  values are zero in our case. It is also seen in Figure 4 that there are three peaks

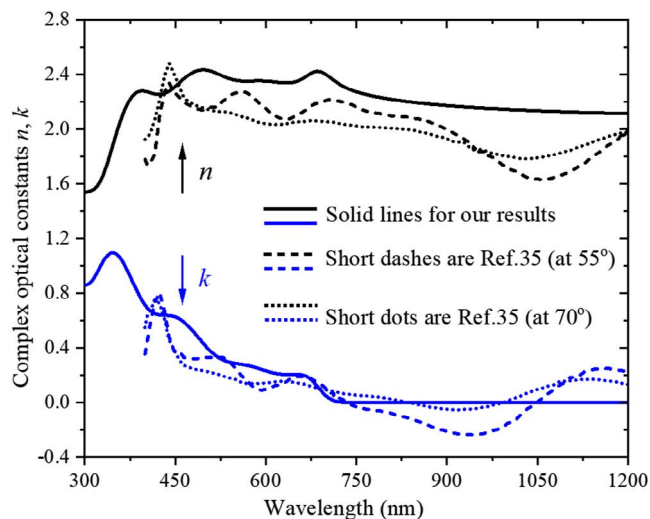


**Figure 4.** The experimentally determined refractive index  $n$  and extinction coefficient  $k$  of the present air-stable  $\text{CsPbI}_3$  thin film in the wavelength range of 300–1200 nm. For comparison, the angle-dependent  $n$  and  $k$  values (at  $55^\circ$  and  $70^\circ$ ) reported in ref. [35] are plotted.

of  $n$  and  $k$  curves in our case, which show a very similar feature to a reported well-known  $\text{CH}_3\text{NH}_3\text{PbI}_3$  perovskite thin film.<sup>[29]</sup> The three peaks are three oscillators.<sup>[29,37]</sup> The three absorption peaks of the extinction coefficient at around 347, 452, and



667 nm correspond to the three exciton transition energies of 3.57, 2.74, and 1.86 eV, respectively.<sup>[29,37]</sup> Because the two quantities of  $n$  and  $k$  are not independent each other, when the  $k$  values are determined, the  $n$  values can be obtained through the Kramers–Kronig relationship (vice versa), which can cause peak difference between  $n$  and  $k$ , as shown in Figure 4. This phenomenon is also found in previous reports.<sup>[29,37]</sup>

To investigate the reliability and repeatability of our complex optical constants as shown in Figure 4, three perovskite samples exhibiting different thicknesses and degrees of surface roughness were measured on the Yiguang instrument. The variation of the obtained  $n$  and  $k$  values is less than 2% due to the uncertainty, compared with our results of Figure 4. In addition, we have also conducted the measurements based on the Sentech instrument, where a large beam spot size of 2–4 mm in a diameter was involved and a longer measurement time of 12–15 min was taken at three angles of 50°, 55°, and 60° (the VASE measurements on the Yiguang instrument at five angles of 43.9°, 48.9°, 53.9°, 58.9°, and 63.9° were finished in a fully automatic way, which took only 3 min). It is found that the complex optical constants exhibit a good agreement with the results from the Yiguang measurement (the variation is less than 3%), as shown in Figure S1, Supporting Information. This indicates that the present  $n$  and  $k$  results are highly reliable as an excellent consistency is shown regardless of specific samples, incident angles, and instruments. The present results of the complex optical constants can be used to help developing high-performance the CsPbI<sub>3</sub> perovskite-based optoelectronic devices including high-efficiency CsPbI<sub>3</sub>/c-Si tandem solar cells through design and simulation.

Air-stable inorganic CsPbI<sub>3</sub> perovskite thin films were prepared. VASE measurements were conducted at five angles (43.9°, 48.9°, 53.9°, 58.9°, and 63.9°) and the ellipsometric parameters were obtained. To fit the data, the model of the perovskite thin film with nonuniform thickness was adopted, where one T–L oscillator and four Gau oscillators were used to describe the bulk CsPbI<sub>3</sub> thin film and the EMA with the voids of 50% was used to describe the surficial roughness. As a result, the experimental complex optical constants of the CsPbI<sub>3</sub> thin film were obtained in the wavelength range of 300–1200 nm. The variation of the obtained complex optical constants was assessed based on different samples and instruments. As a result, a high repeatability was obtained. The present results have opened the door to conduct design and simulations on the photovoltaics devices based on air-stable CsPbI<sub>3</sub> thin films including high-efficiency CsPbI<sub>3</sub>/c-Si tandem solar cells.

## Experimental Section

**Preparations:** CsPbI<sub>3</sub> perovskite thin films were deposited through one-step deposition method. The precursor solution was prepared by dissolving 1 M PbI<sub>2</sub>, 1 M CsI (99.9%, Sigma), and 1 M dimethylammonium iodide (DMAI; purity > 99.9%, Dyesol) in dimethylformamide (DMF, purity > 99%, Sigma) solvent at room temperature. The solution was spin-coated on the glass substrate that has been preheated to 70 °C at 2000 rpm for 20 s. Then, the samples were annealed at 200 °C to obtain CsPbI<sub>3</sub> perovskite thin films, followed by cooling at room temperature. During annealing, most of DMAI molecules would be evaporated and finally, the main composition was CsPbI<sub>3</sub> perovskite. The deposition processes were conducted in dry air (humidity is between 10% and 20%).

**Characterizations:** To investigate the crystalline structure, the XRD spectra of inorganic perovskite CsPbI<sub>3</sub> thin films on glass substrate were conducted using an X-ray diffractometer (Philips PW-1830) equipped with X-ray tube Cu K $\alpha$  radiation. The absorbance spectrum of the CsPbI<sub>3</sub> thin film on the glass substrate was measured from the CsPbI<sub>3</sub> side using a spectrophotometer (Perkin Elmer Lambda 20) to determine the optical bandgap. The PL spectrum was measured with calibrated CCS200 spectrometer (Thorlabs) using 75 mW laser with the wavelength of 405 nm for excitation. The laser beam was focused and directed into an integrating sphere (Labsphere) with a diameter of 15 cm. An optical fiber with a diameter of 1 mm (FP1000URT, Thorlabs) was used for collection of the emission from the integrating sphere. Integration time of 60 s was used for the collection of PL emission. The spectral response of the whole detection system was calibrated using a calibration lamp (HL-3plus-INT-CAL, Ocean Optics). SEM (Zeiss Supra 60VP) images were obtained to assess the cross-sectional morphology and thickness. Optical profiler (Bruker Contour GT-K) was used to measure CsPbI<sub>3</sub> surface profile. An AFM (Bruker Dimension Icon) was used to investigate surface roughness of the sample. Ellipsometry measured a change in polarization as light reflected from the sample of CsPbI<sub>3</sub> thin film. This polarization change was represented as an amplitude ratio,  $\Psi$ , and the phase difference,  $\Delta$ . The CsPbI<sub>3</sub> perovskite thin film samples were measured on the ellipsometer (China Yiguang) at five variable angles of 43.9°, 48.9°, 53.9°, 58.9°, and 63.9° to obtain the values of  $\Psi$  and  $\Delta$ . The VASE measurements were conducted directly after CsPbI<sub>3</sub> film deposition and the measurements were completed within  $\approx$ 3 min. The size of beam spot was  $\approx$ 200  $\mu$ m in diameter.

**Models and Fitting:** For ellipsometric parameters  $\Psi$  and  $\Delta$  can be related to the ratio of Fresnel reflection coefficients  $R_p$  and  $R_s$  for p- and s-polarized light, respectively, as described in Equation (1)

$$\rho = \frac{R_p}{R_s} = \tan(\Psi)e^{i\Delta} \quad (1)$$

The VASE technique measured the ratio of the two values and therefore the measured results were highly accurate and reproducible.<sup>[38]</sup> To construct a model of the sample and fit the experimental data ( $\Psi$  and  $\Delta$ ), a commercial software package (WVASE32 v.3.888, J. A. Woollam) was used. The present sample structure was a perovskite thin film on a glass substrate. The Cauchy dispersion function was used to describe the property of glass substrate. For the perovskite thin film, it was divided into two parts: one was bulk planar perovskite layer (this thickness was defined as  $d_{\text{bulk}}$ ) and the other was a thin surficial layer with a certain roughness (the surface roughness was defined as  $d_{\text{rough}}$ ). The oscillators such as T–L and Gau were successfully used to describe the dielectric function of the perovskites.<sup>[29–33]</sup> The T–L oscillator function and Gau oscillator function are expressed in Equation (2) and (4), respectively.<sup>[38]</sup>

$$\epsilon_{n-T-L} = \epsilon_{n1} + i\epsilon_{n2} \quad (2)$$

where, when  $E < E_{gn}$ ,  $\epsilon_{n2} = 0$ ; and when  $E > E_{gn}$ ,

$$\epsilon_{n2} = \left[ \frac{A_n E_{0n} C_n (E - E_{gn})^2}{(E^2 - E_{0n}^2)^2 + C_n^2 E^2} \times \frac{1}{E} \right] \quad (3)$$

In Equation (2), the subscript T–L indicates that the model is based on the Tauc joint density of states and the Lorentz oscillator. The four fitting parameters are  $A_n$ ,  $E_{0n}$ ,  $C_n$ , and  $E_{gn}$ , where these parameters are in units of energy of eV and used for the WVASE fitting.

$$\epsilon_{n-Gau} = \epsilon_{n1} + i\epsilon_{n2} \quad (4)$$

where

$$\epsilon_{n1} = \frac{2}{\pi} P \int_0^{\infty} \frac{\xi \epsilon_{n2}(\xi)}{\xi^2 - E^2} d\xi \quad (5)$$

$$\epsilon_{n2} = A_n e^{-\left(\frac{E-E_n}{\sigma}\right)^2} - A_n e^{-\left(\frac{E+E_n}{\sigma}\right)^2} \quad (6)$$

$$\sigma = \frac{B_{rn}}{2\sqrt{\ln(2)}} \quad (7)$$

In Equation (4), the subscript Gau indicates that the model is based on the Gaussian oscillator. The three fitting parameters are  $A_n$  (dimensionless),  $E_n$  (eV), and  $B_{rn}$  (eV), where the three parameters are used for the WVASE fitting.

The Bruggeman EMA is usually suitable to describe rough perovskite surficial layer, where the medium consists of the mixture of  $x\%$  air void and  $(100 - x)\%$  perovskite material, where  $x$  can take a value in the range from 0 to 100. When a perovskite thin film does not have parallel interfaces, a nonideal model of thickness nonuniformity should be considered for model construction, where it can be implemented at “model options” of the WVASE. This thickness nonuniformity is simulated by calculating data for the structure using a series of slightly different thickness for perovskite layer in the model. The commercial software package (WVASE32 v.3.888, J. A. Woollam) offers three convolution profile shapes (square, triangular, and Gaussian) for the structure.

## Supporting Information

Supporting Information is available from the Wiley Online Library or from the author.

## Acknowledgements

W.Y. thanks the financial support from the German Research Foundation (DFG) (Ref. YA516/1-1). This work was partly carried out with support of the Karlsruhe Nano Micro Facility (KNMF) at Karlsruhe Institute of Technology (KIT). The technical support from the KNMF includes AFM, Bruker Contour GT-K, and SEM. W.Y. greatly thanks the Yiguang Instrument Co. of China for providing ellipsometric measurements and technical support. The authors thank Dr. Ulrich W. Paetzold, Dr. Kunyuan Xu, and Dr. Dmitry Busko for useful discussions and technical support. H.C. thanks the Beijing Natural Science Foundation (grant no. 2182031) and the financial support from the National Natural Science Foundation of China (grant no. 21875013). B.S.R. would like to acknowledge the financial support provided by the Helmholtz Association: 1) a Helmholtz Recruitment Initiative Fellowship; 2) the research program Science and Technology of Nanosystems (STN); and 3) the Helmholtz Energy Materials Foundry (HEMF).

## Conflict of Interest

The authors declare no conflict of interest.

## Keywords

air-stable CsPbI<sub>3</sub>, complex optical constants, ellipsometry, inorganic perovskites, thin films

Received: February 10, 2020  
Revised: March 18, 2020  
Published online: April 7, 2020

- [1] A. Kojima, K. Teshima, Y. Shirai, T. Miyasaka, *J. Am. Chem. Soc.* **2009**, *131*, 6050.  
[2] NREL, Best Research-Cell Efficiency Chart, <https://www.nrel.gov/pv/cell-efficiency.html> (accessed: April 2019).  
[3] M. Kulbak, D. Cahen, G. Hodes, *J. Phys. Chem. Lett.* **2015**, *6*, 2452.

- [4] R. J. Sutton, G. E. Eperon, L. Miranda, E. S. Parrott, B. A. Kamino, J. B. Patel, M. T. Hörlantner, M. B. Johnston, A. A. Haghighirad, D. T. Moore, H. J. Snaith, *Adv. Energy Mater.* **2016**, *6*, 1502458.  
[5] R. E. Beal, D. J. Slotcavage, T. Leijtens, A. R. Bowring, R. A. Belisle, W. H. Nguyen, G. F. Burkhard, E. T. Hoke, M. D. McGehee, *J. Phys. Chem. Lett.* **2016**, *7*, 746.  
[6] J. Lei, F. Gao, H. X. Wang, J. Li, J. X. Jiang, X. Wu, R. R. Gao, Z. Yang, S. Z. (Frank) Liu, *Sol. Energy Mater. Sol. Cells* **2018**, *187*, 1.  
[7] H. W. Yuan, Y. Y. Zhao, J. L. Duan, Y. D. Wang, X. Y. Yang, Q. W. Tang, *J. Mater. Chem. A* **2018**, *6*, 24324.  
[8] X. Y. Liu, X. H. Tan, Z. Y. Liu, H. B. Ye, B. Sun, T. L. Shi, Z. R. Tang, G. L. Liao, *Nano Energy* **2019**, *56*, 184.  
[9] Y. Y. Zhao, T. S. Liu, F. M. Ren, J. L. Duan, Y. D. Wang, X. Y. Yang, Q. H. Li, Q. W. Tang, *Mater. Chem. Front.* **2018**, *2*, 2239.  
[10] Y. Wang, M. I. Dar, L. K. Ono, T. Y. Zhang, M. Kan, Y. W. Li, L. J. Zhang, X. T. Wang, Y. G. Yang, X. Y. Gao, Y. B. Qi, M. Grätzel, Y. X. Zhao, *Science* **2019**, *365*, 591.  
[11] A. Swarnkar, A. R. Marshall, E. M. Sanehira, B. D. Chernomordik, D. T. Moore, J. A. Christians, T. Chakrabarti, J. M. Luther, *Science* **2016**, *354*, 92.  
[12] T. Zhang, M. I. Dar, G. Li, F. Xu, N. Guo, M. Grätzel, Y. Zhao, *Sci. Adv.* **2017**, *3*, e1700841.  
[13] W. Ahmad, J. Khan, G. Niu, J. Tang, *Sol. RRL* **2017**, *1*, 1700048.  
[14] Q. Wang, X. Zheng, Y. Deng, J. Zhao, Z. Chen, J. Huang, *Joule* **2017**, *1*, 371.  
[15] C. F. J. Lau, X. Deng, J. Zheng, J. Kim, Z. Zhang, M. Zhang, J. Bing, B. Wilkinson, L. Hu, R. Patterson, S. Huang, *J. Mater. Chem. A* **2018**, *6*, 5580.  
[16] S. Xiang, W. Li, Y. Wei, J. Liu, H. Liu, L. Zhu, H. Chen, *Nanoscale* **2018**, *10*, 9996.  
[17] G. E. Eperon, G. M. Paterno, R. J. Sutton, A. Zampetti, A. A. Haghighirad, F. Cacialli, H. J. Snaith, *J. Mater. Chem. A* **2015**, *3*, 19688.  
[18] S. S. Xiang, Z. H. Fu, W. P. Li, Y. Wei, J. M. Liu, H. C. Liu, L. Q. Zhu, R. F. Zhang, H. N. Chen, *ACS Energy Lett.* **2018**, *3*, 1824.  
[19] Y. Wang, T. Y. Zhang, M. Kan, Y. X. Zhao, *J. Am. Chem. Soc.* **2018**, *140*, 12345.  
[20] K. Wang, Z. W. Jin, L. Liang, H. Bian, D. L. Bai, H. R. Wang, J. R. Zhang, Q. Wang, S. Z. Liu, *Nat. Commun.* **2018**, *9*, 4544.  
[21] M. Jaysankar, M. Filipič, B. Zielinski, R. Schmager, W. Song, W. M. Qiu, U. W. Paetzold, T. Aernouts, M. Debucquoy, R. Gehlhaar, J. Poortmans, *Energy Environ. Sci.* **2018**, *11*, 1489.  
[22] M. van Eerden, M. Jaysankar, A. Hadipour, T. Merckx, J. J. Schermer, T. Aernouts, J. Poortmans, U. W. Paetzold, *Adv. Opt. Mater.* **2017**, *5*, 1700151.  
[23] J. Lehr, M. Langenhorst, R. Schmager, S. Kirner, U. Lemmer, B. S. Richards, C. Case, U. W. Paetzold, *Sustainable Energy Fuels* **2018**, *2*, 2754.  
[24] D. A. Jacobs, M. Langenhorst, F. Sahli, B. S. Richards, T. P. White, C. Ballif, K. R. Catchpole, U. W. Paetzold, *J. Phys. Chem. Lett.* **2019**, *10*, 3159.  
[25] M. S. Alias, I. Dursun, D. Shi, M. I. Saidaminov, E. M. Diallo, D. Prianteand, T. K. Ng, O. M. Bakr, B. S. Ooi, *Vac. Sci. Technol. B* **2015**, *33*, 051207.  
[26] M. S. Alias, Y. Yang, T. K. Ng, I. Dursun, D. Shi, M. I. Saidaminov, D. Priante, O. M. Bakr, B. S. Ooi, *J. Phys. Chem. Lett.* **2016**, *7*, 137.  
[27] I. Suárez, E. J., Juárez-Pérez, J. Bisquert, I. Mora-Seró, J. P. Martínez-Pastor, *Adv. Mater.* **2015**, *27*, 6157.  
[28] P. Brenner, O. Bar-On, M. Jakob, I. Allegro, B. S. Richards, U. W. Paetzold, I. A. Howard, J. Scheuer, U. Lemmer, *Nat. Commun.* **2019**, *10*, 988.  
[29] P. Löper, M. Stuckelberger, B. Niesen, J. Werner, M. Filipič, S.-J. Moon, J.-H. Yum, M. Topič, S. De Wolf, C. Ballif, *J. Phys. Chem. Lett.* **2015**, *6*, 66.

- [30] Y. J. Jiang, M. A. Green, R. Sheng, A. Ho-Baillie, *Sol. Energy Mater. Sol. Cells* **2015**, *137*, 253.
- [31] M. S. Alias, I. Dursun, M. I. Saidaminov, E. M. Diallo, T. K. N. G. P. Mishra, O. M. Bakr, B. S. Ooi, *Opt. Express* **2016**, *24*, 16587.
- [32] C. W. Chen, S. Y. Hsiao, C. Y. Chen, H. W. Kang, Z. Y. Huang, H. W. Lin, *J. Mater. Chem. A* **2015**, *3*, 9152.
- [33] Z. A. Xie, S. R. Sun, Y. Yan, L. L. Zhang, R. X. Hou, F. Y. Tian, G. G. Qin, *J. Phys.: Condens. Matter* **2017**, *29*, 245702.
- [34] M. L. Zhao, Y. J. Shi, J. Dai, J. Lian, *J. Mater. Chem. C* **2018**, *6*, 10450.
- [35] R. K. Singh, R. Kumar, N. Jain, S. R. Dash, J. Singh, A. Srivastava, *J. Taiwan Inst. Chem. Eng.* **2019**, *96*, 538.
- [36] C. F. J. Lau, Z. P. Wang, N. Sakai, J. H. Zheng, C. H. Liao, M. Green, S. J. Huang, H. J. Snaith, A. Ho-Baillie, *Adv. Energy Mater.* **2019**, *9*, 1901685.
- [37] Z. Xie, S. R. Sun, Y. Yan, L. L. Zhang, R. X. Hou, F. Y. Tian, G. G. Qin, *J. Phys.: Condens. Matter* **2017**, *29*, 245702.
- [38] J. A. Woollam ellipsometry solutions, Guide to using WVASE spectroscopic ellipsometry data acquisition and analysis software, <https://www.jawoollam.com> (accessed: December 2019).